Available online at www.sciencedirect.com

jmr&t Journal of Materials Research and Technology

journal homepage: www.elsevier.com/locate/jmrt

# Microstructure, segregation and mechanical properties of A356 alloy components fabricated by rheo-HPDC combined with the swirled enthalpy equilibration device (SEED) process

Guo-chao Gu [a,b,c,*], Li-xin Xiang [a,b], Rui-fen Li [d], Hong-liang Zheng [a,b], Yu-peng Lu [a,b,**], Raphaël Pesci [e]

[a] Key Laboratory for Liquid-Solid Structural Evolution and Processing of Materials, Ministry of Education, Shandong University, Jinan 250061, Shandong, PR China

[b] School of Materials Science and Engineering, Shandong University, Jinan 250061, Shandong, PR China

[c] Suzhou Institute of Shandong University, Suzhou, Jiangsu, 215123, PR China

[d] Shandong Institute for Product quality inspection, Jinan 250102, PR China

[e] ENSAM-Arts et Métiers Sciences and Technologies, LEM3 UMR CNRS 7239, 4 Rue Augustin Fresnel, Metz Cedex 3, 57078, France

ARTICLE INFO

*Article history:*
Received 18 June 2023
Accepted 15 September 2023
Available online 19 September 2023

*Keywords:*
A356
Rheo-HPDC
Segregation
Microstructure
Mechanical property

ABSTRACT

The challenges commonly associated with conventional high pressure die casting (HPDC) have led to increased interest in semi-solid metal (SSM) forming processes. In the present study, semi-solid slurries of A356 alloy prepared by the Swirled Enthalpy Equilibration Device (SEED) process were used for manufacturing components with complex shape by using a high pressure die casting machine. The segregation phenomenon and the effect of heat treatment on the microstructure evolution and mechanical properties were investigated. The results showed that the alloy consists of primary spherical α-Al grains, secondary solidified α-Al grains, eutectic Si, iron-rich intermetallic phases and low porosities. The microstructural investigations revealed that the eutectic Si particles underwent fragmentation, spheroidization and coarsening with increasing solution temperature. Furthermore, the solution treatment results in the dissolution of the π-$Al_8FeMg_3Si_6$ phase and the growth of the β-$Al_5FeSi$ phase. The hardening peaks at 170 °C could be obtained with ageing for 5 h. Due to both solution and precipitation strengthenings, the yield strength, ultimate tensile strength and hardness of A356 alloy after heat treatment increase significantly compared to those in the as-rheocast state: they reach 266 MPa, 343 MPa and 110 $HV_{0.2}$, respectively. The analysis of fracture surfaces of rheo-HPDC samples in both the as-rheocast and the heat-treated states revealed a mixed mechanism of dimples and quasi-cleavage. The microstructure inside the part was found to be quasi-homogeneous while the segregation phenomenon in different zones of the part is affected by die geometry during the filling process. The results imply that the SEED-HPDC

* Corresponding author. Key Laboratory for Liquid-Solid Structural Evolution and Processing of Materials, Ministry of Education, Shandong University, Jinan 250061, Shandong, PR China.

** Corresponding author. Key Laboratory for Liquid-Solid Structural Evolution and Processing of Materials, Ministry of Education, Shandong University, Jinan 250061, Shandong, PR China.

E-mail addresses: guochaogu@sdu.edu.cn (G.-c. Gu), biosdu@sdu.edu.cn (Y.-p. Lu).

https://doi.org/10.1016/j.jmrt.2023.09.153

process has the potential to be industrialized by implementing appropriate heat treatments for producing complex components with good mechanical properties.



## 1. Introduction

The increasing demand to produce lightweight and durable automotive parts has a significant effect on the selection of materials. Al-Si-Mg alloys are considered to be excellent candidate materials for automotive applications, because of their high strength-to-weight ratio, good castability and good corrosion resistance [1]. However, the microstructure and mechanical properties of as-cast components largely depends on casting and heat treatment processes. Generally, the microstructure of the as-cast components mainly consists of primary α-Al dendrites, inter-dendritic irregular Al-Si eutectic phases and other intermetallic phases. The coarse and irregular intermetallics as well as acicular Al-Si phase could decrease the stress cracking resistance, resulting in poor ductility and low strength [2]. These detrimental effects can be controlled by suitable casting process and/or heat treatment processes.

Compared with conventional high pressure die casting (HPDC) process, semi-solid metal (SSM) forming as well as the heat treatment could improve the strength while preserving the high ductility of SSM components by modifying the morphology of formed phases and intermetallics, which are homogeneously distributed in the matrix [3,4]. In addition, the laminar flow of semi-solid metal during die-filling could reduce the level of entrapped gas and the shrinkage problems during solidification, thereby avoiding blistering caused by gas expansion during heat treatment at elevated temperature. Consequently, semi-solid metal process has been considered a valid alternative for producing sound Al-Si-Mg automotive light-weight parts, such as control arms, engine brackets, etc. [5]. Nowadays, between the two main routes (rheo-casting and thixo-casting) following the SSM process, the rheo-casting approach holds the promise of being more cost effective than thixo-casting, because of unnecessary specialized feedstock preparation and reusable of returns/scraps [6]. Researchers have used various semi-solid slurry preparation methods and combined with HPDC process to prepare products with good performance, such as gas induced semi-solid process (GISS) [7], cooling slope [8], ultrasonic vibration process (USV) [9], etc. The swirled enthalpy equilibrium device (SEED) [10] is a simple, reliable, and cost-effective slurry preparation method which allows producing components with a wide range of aluminum alloys, such as A356, A201, 2618, 6063 and 7075 [11]. Additionally, it requires minimum control while offering a relatively large operating window. Based on rapid and controlled thermal equilibrium between a metallic crucible and the bulk of molten aluminum by mechanical agitation, the semi-solid slurry with desired microstructure can be obtained with proper process parameters. Liang [12] studied the influence of SEED process parameters on microstructure of the A357 alloy and stated that the fine and round microstructure could be obtained at low pouring temperature. It was also found that the microstructure of the slurry with low apparent viscosity could be refined by higher convection strength resulted from increasing eccentric speed. In addition, with the increase of swirl duration, the small grains would dissolve, while big size grains keep growing via the Ostwald ripening mechanism. In order to further improve the efficiency of SEED process, the process and equipment were optimized at General Research Institute for Nonferrous Metals (GRINM GROUP, China), based on deep understanding of thermodynamics and kinetic mechanisms of solidification process during the slurry preparation [13]. The modified SEED process can significantly decrease the radial temperature gradient of the melt because of the slow cooling rates, facilitating more uniform slurry and more spherical microstructure. Based on the achievements above mentioned, the SEED process was applied for the semi-solid slurry preparation in this study.

Heat treatment is considered as an important operation to obtain a good combination of strength and ductility of aluminum casting components. The typical heat treatment procedure applied to Al-Si-Mg alloys is T6 or T7, which consists of solution treatment and quenching followed by artificial ageing at different temperatures and times. However, the different microstructure and solidification history of SSM components indicate that heat treatment conditions which were optimized for conventionally cast materials may not applicable to SSM components [14]. Investigations on the microstructure evolution and mechanical properties of semi-solid Al-Si-based alloys have been performed [15–17]. The results show that homogenization of microstructure, fragmentation and spheroidization of eutectic Si and fine precipitates after heat treatment improve the mechanical properties of alloys. However, the fraction, distribution and morphology of the common intermetallic compounds (especially the iron-rich intermetallics) during semi-solid forming process, which may result in inferior mechanical properties [1], are less investigated.

The industrial fabrication of aluminum alloys components with good mechanical properties and low cost remains a significant target for rheo-casting process. The heat treatment optimization and material flow behavior have been frequently reported by using relatively small samples processed with simple die geometries. Therefore, the rheo-casting process for further automotive component fabrication requires further study. The aim of this study is to develop a rheo-HPDC process for the fabrication of automotive limit block components for further industrial application. The components were formed through a HPDC machine on a commercial A356 alloy prepared using the SEED process. The microstructure evolution and the mechanical properties of the components were

investigated as a function of different heat treatment parameters. In addition, the surface liquid segregation was also analyzed and discussed.

## 2. Experimental methods

The material used for producing automotive components was a commercial A356 aluminum alloy with a chemical composition of 6.45% Si, 0.41% Mg, 0.13% Fe, 0.007% Mn, 0.098% Cu, 0.05% Ti and Al balanced by mass, determined by a LAB M12 direct reading spectrometer (SPECTRO, Germany);. The solidus and liquidus temperatures of the alloy were 559.5 °C and 614.8 °C, respectively, which were obtained by DSC tests. The DSC samples of about 3 mm in diameter and 15.24 mg were tested by using a NETZSCH-404c (NETZSCH, Germany) differential scanning calorimeter. The samples were heated to 700 °C and then cooled to room temperature at 10 °C/min. The solidus and liquidus temperatures were determined by using tangent method, as outlined by the International Confederation for Thermal Analysis (ICTA).

The alloy of 100 kg was remelted at 720 °C in a resistance furnace (SR2-25, Jiande Xin'anjiang Electric Control Equipment Co., Ltd., China) and N-degassed for 30 min. Then the master alloy (Al-5Ti-B) of 855 g was added into the melt at 690 °C for grain size refinement. After holding at 620 °C in the furnace, the melt of ~2.2 kg was transferred by means of a ladle and poured into a preheated steel vessel (inner diameter of 78 mm) in order to get sufficient cooling of the melt to the desired solid fraction and avoid thermal shock. During the SEED process [11], the primary solid phase generated at the walls of the vessel was evenly distributed throughout the vessel due to the eccentricity of the swirl motion. After swirling for 100 s at a rate of 150 rpm, the semi-solid slurry (~585 °C) was transferred to the shoot sleeve of a HPDC machine (SC-N/34, Buhler, Switzerland). The slurry was then injected into the die cavity, with the plunger velocity of the HPDC machine being lower than 1 m/s during the filling process. A pressure of ~800 bar was applied and held for 20 s after the injection to ensure high-integrity castings.

Following the rheo-HPDC process, the components underwent heat treatment under specific conditions. The solution treatment was conducted in an electric furnace at 540 °C (proposed by ASTM B 917), with temperature control of ±1 °C, for various holding times and then quenched in water at 60 °C. The quenched components were then aged for different durations, ranging from 2 to 9 h, at 170 °C.

Some tensile and microhardness samples were electrodischarge-machined from the components (shown in Fig. 1). Vickers hardness values were determined by using MH-3 (Shanghai Hengyi Precision Instrument Co., Ltd., China) from the average of eight readings per sample by applying a load of 200 gf and a dwell time of 15 s on polished samples following standard GB/T 4340.1–2009. The dog-bone tensile samples with a gauge length of 38 mm and 6 mm in diameter were tested according to GB/T 228.1–2010 by using a universal material testing machine (Zwick-Z250, ZwickRoell, German) with a constant strain rate of $4.40^{-4}$ $s^{-1}$ at room temperature to obtain the tensile strength and elongation of the samples.

A microstructural characterization in various zones was conducted using an optical microscope (Nikon LV100ND, Nikon, Japan) and scanning electron microscope (SEM, SU-70, Hitachi, Japan) after mechanical polishing and etching (Keller's agent). An electron probe micro analyzer (EPMA, JXA-8530F PLUS, JEOL Ltd., Japan) and a transmission electron microscope (TEM, Talos F200X, FEI, America) with an

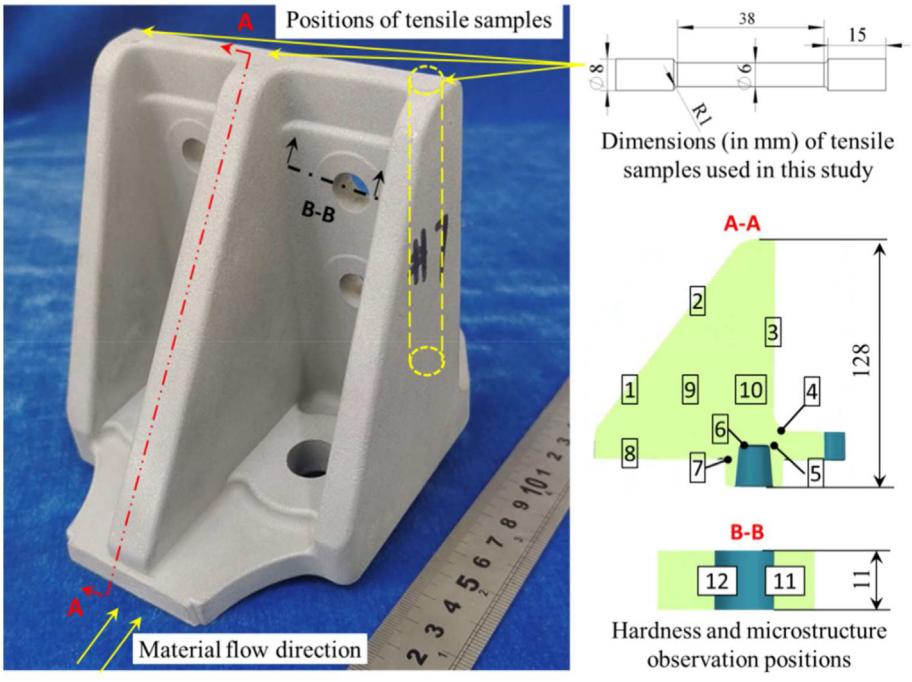


**Fig. 1 – Rheo-HPDC component: the samples were taken at various locations for mechanical tests and microstructure observations.**

acceleration voltage of 200 kV were used to observe secondary phases and elements distribution. Quantitative image analysis was performed by using ImageJ software (V1.8.0; National Institutes of Health, Bethesda, MD, USA). The solid fraction ($F_s$) was estimated by measuring the volume fraction of the large light gray α-Al grains, which were preserved during quenching from semi-solid state. The average grain size (*D*) and average shape factor (*F*) were determined by using the equations as follows (Eq. (1) and Eq. (2)). The procedure for the estimations was detailed in Ref. [18]. In addition, point counting method (GB/T 15749-2008) was used to obtain static results of the Fe-rich intermetallic compounds.

$$D = \frac{\Sigma_{i=1}^{N}\sqrt{4A_i/\pi}}{N} \quad (1)$$

$$F = \frac{\Sigma_{i=1}^{N}\sqrt{4A_i}}{P_i^2} \quad (2)$$

Where $A_i$ is the area grains, $P_i$ is the perimeter of grains, *N* and i are the number of grains.

## 3. Results

### 3.1. *Materials in as-rheocast state*

Non-destructive X-ray technique was used to assess the internal soundness of the formed parts. Fig. 2 compares the X-ray radiographs of components produced using conventional HPDC and rheo-HPDC process. The results indicate that the parts produced by conventional HPDC contained large amounts of white zones (Fig. 2(a)), which were identified as voids. The porosity was attributed to the turbulent die-filling in conventional HPDC. Furthermore, the laminar flow during the die-filling of rheo-HPDC nearly eliminates gas entrapment (Fig. 2(b)) and reduces shrinkage problems during solidification.

The microstructure of the rheo-HPDC component at different positions (described in Fig. 1) are shown in Fig. 3. The microstructure exhibits the typical structure of rheo-cast Al-Si alloy, which is composed of spherical or rosette-like primary α-Al grains (average grain size of ~90 μm, and shape factor of ~0.76) in light gray surrounded by the eutectic network in dark gray and secondary α-Al grains in light gray. The spheroidization of primary α-Al grains in SEED process results from the combined effect of the processing parameters. Upon pouring the melt into the steel vessel, a large number of nuclei would form on the vessel wall as a result of the rapid cooling. The grains formed on the vessel wall can be dissociated by necking and enter the melt due to the strong liquid convection [19]. At this time, the volume fraction of primary α-Al grains increases quickly and then stabilizes because of the thermal equilibrium between the vessel and its contents. The SEED process results in relatively homogeneous composition and temperature fields, which limits the constitutional undercooling and thereby leads to globular growth of α-Al grains. Qu et al. [20] further studied the microstructural evolution mechanism of the SEED process by using Phase-Field-Lattice-Boltzmann scheme and stated that the morphology evolution during semi-solid slurry preparation by SEED process was determined by the interaction between thermal-solute diffusion and solid-liquid interface migration during solidification.

Besides the spherical and rosette-like grains, fine dendrites or equiaxed grains are also observed, as presented in Fig. 3. These fine grains (secondary α-Al grains) were formed from the remaining liquid phase during solidification. During the die filling process, the plunger pushed the primary α-Al grains and liquid phase forward, causing it to enter the cavity through the gate. Subsequently, the primary α-Al grains underwent further evolution while the remaining liquid phase underwent secondary solidification and eutectic reaction within the die cavity, leading to the formation of secondary α-Al and eutectic phases. The cooling rate played a crucial role in determining the morphology of the grains, with fine equiaxed and dendritic grains being formed depending on the cooling rate. Liu et al. [21] also reported similar solidification characteristics of Al-8Si-0.5Fe produced by rheo-diecasting process. In addition, some voids were observed in the alloy (Fig. 3), with a porosity around 0.12%. It was also found that the voids mainly distributed at the interface between the liquid and the primary α-Al grains and were small shrinkage pores. Secondary phases are observed by EPMA, as shown in Fig. 4. Coral-like eutectic Si phases and primary Si particles with sharp edges and corners were observed, as shown in Fig. 4(a). In addition, as-rheocast microstructures showed intermetallic phases, which could be π-$Al_8FeMg_3Si_6$, β-$Al_5FeSi$ and $Mg_2Si$, as

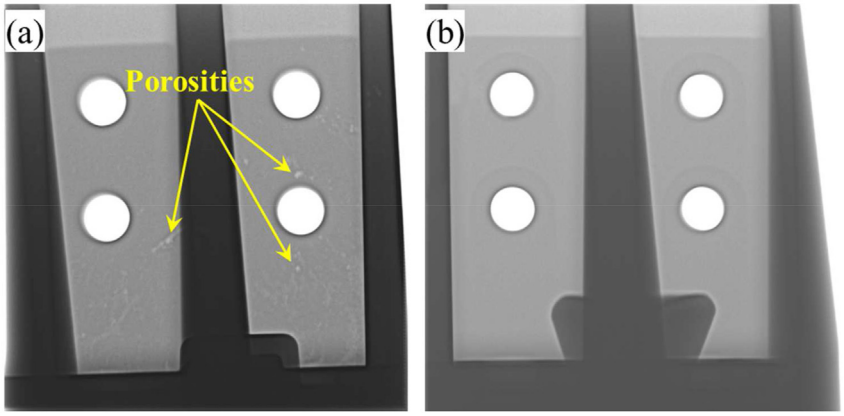


**Fig. 2 – 2D X-ray radiograph of limit block brackets produced by (a) conventional HPDC and (b) rheo-HPDC processes.**

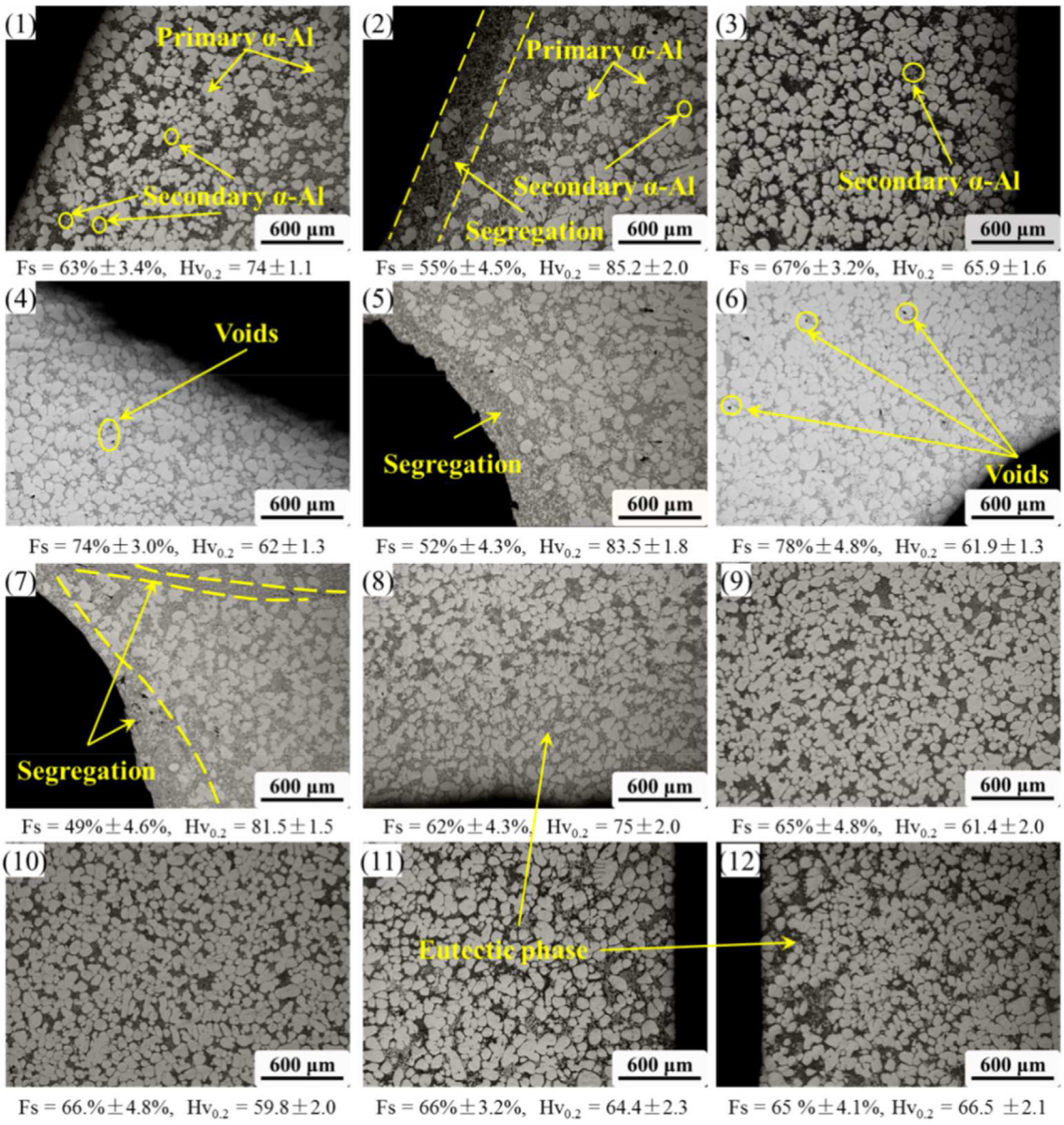


**Fig. 3 – OM images and hardness of as rheo-HPDC alloy in various zones.**

shown in Fig. 4(b–f). The π-$Al_8FeMg_3Si_6$ phase was the dominant phase throughout the range of compositions. Zhao et al. [22] found that for Al-7Si-0.3 Mg alloy, the π-$Al_8FeMg_3Si_6$ phase could easily be observed, while there was little β-$Al_5FeSi$ phase when Fe content is ~0.1 wt% in the permanent mold casting state. Although β-$Al_5FeSi$ phase was not identified by EMPA, there could be some, since the π-$Al_8FeMg_3Si_6$ phase in gray often grows in close association with β-$Al_5FeSi$ phase in black during solidification [23], as shown in Fig. 4(a).

This work studied the variations of both microhardness and solid fraction in different positions, as depicted in Fig. 3. The materials with higher liquid fraction exhibited higher hardness. Payandeh et al. [24] also suggested that the liquid die cast Al-6Si-2Cu-Zn had a higher hardness than the rheo-HPDC ones. This can be attributed to liquid segregation during the rheo-HPDC process, where the former liquid zone comprises a relatively higher eutectic phase enriched in alloying elements. More quantitative results indicate that the solid fraction is about 50% near liquid segregation zones (zones 2, 5 and 7 in Fig. 3). The solid fraction in areas with slight segregation is ~62% (zones 1, 3 and 8and positions 4 and 6 exhibit higher solid fraction (~0.75). However, the microstructure appears to be nearly homogeneous (zones 9 and 10), excepted when considering the segregation zones. This observation is consistent even in areas with obstacles (zones 11 and 12). The heterogeneous flow is attributed to the geometry of the part and the special flow behavior of the semi-solid slurry during die filling, which will be discussed in Section 4.1.

### 3.2. *Microstructure after solution and ageing treatment*

Fig. 5(a–e) shows the change in the morphology of the phases at different solution times. There is no coarsening effect on

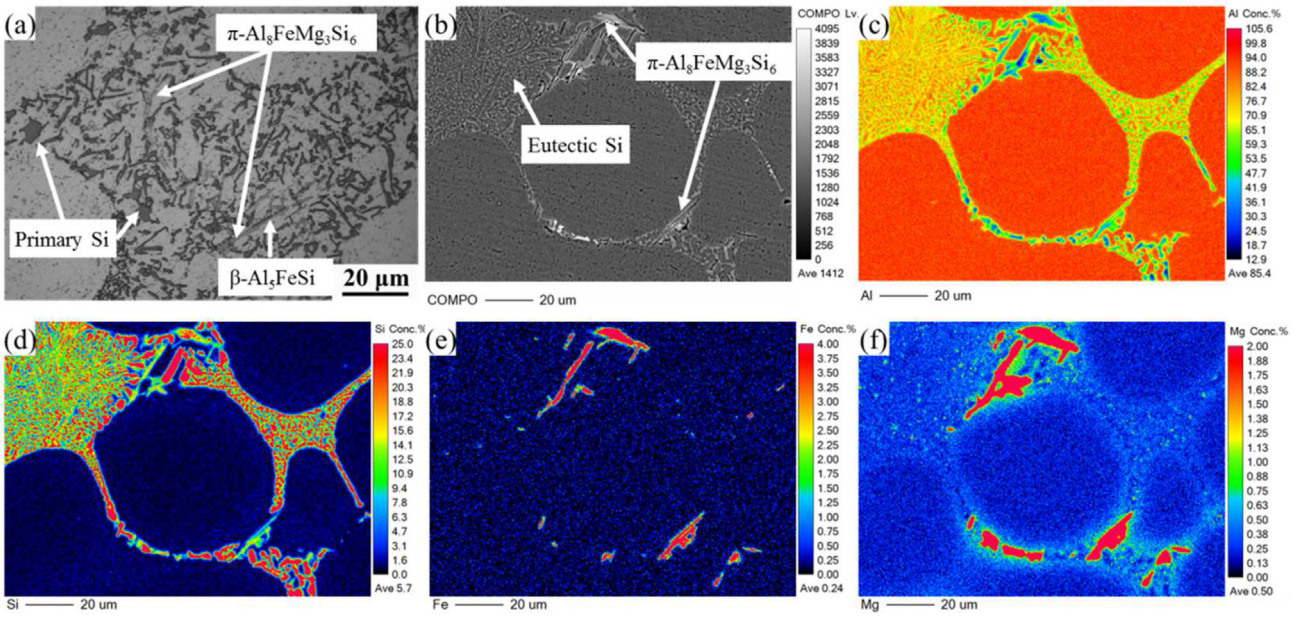


**Fig. 4 – (a) OM image; (b) SEM back-scattered electron image; (c–f) EPMA results of the distribution of Al, Si, Fe and Mg in as-rheocast alloy.**

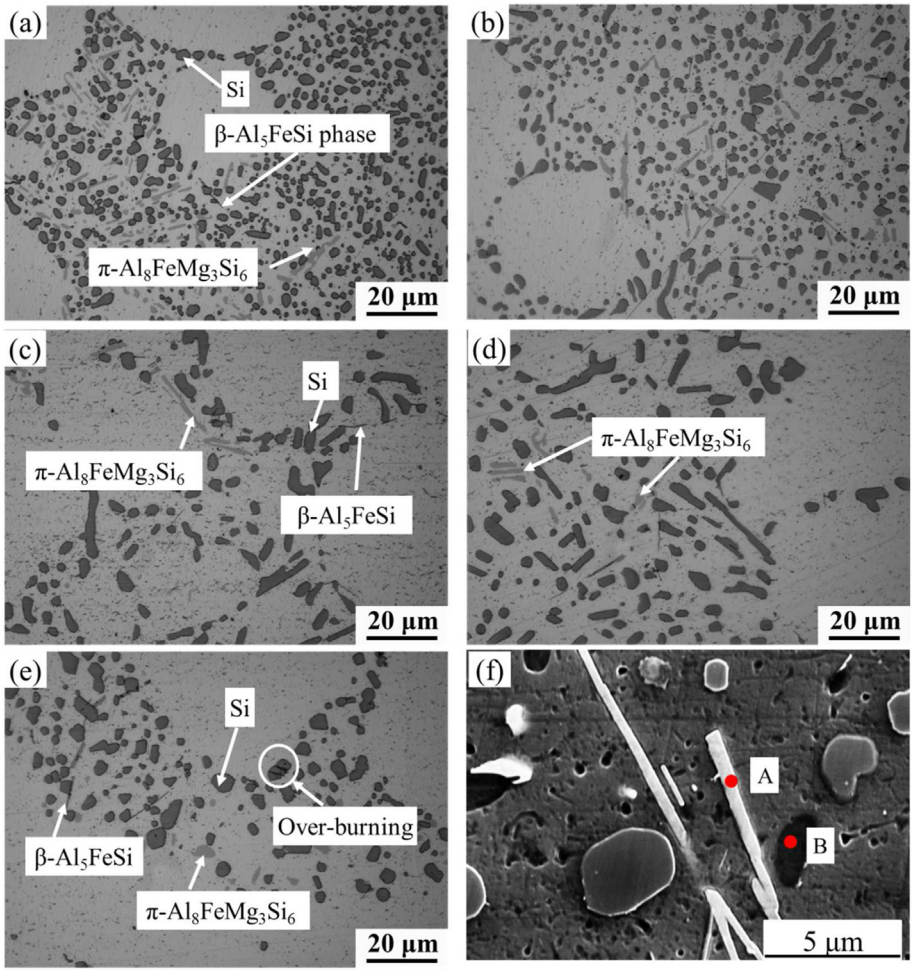


**Fig. 5 – Microstructures of the alloy at 540 °C for different solution time: (a) 1h, (b) 2h, (c) 3h, (d) 5h, (e) 6h and (f) the SEM morphology of the intermetallic phases labeled A and B.**

the α-Al grains, since the solution-treated alloys show a similar size to the as-rheocast condition. However, the secondary phases are considerably modified in size, volume fraction and morphology. The morphology of Si particles can be classified as three stages: fragmentation, spheroidization and coarsening of eutectic Si. As shown in Fig. 5(a) and (b), after 1 and 2 h of solution treatment, the as-rheocast eutectic Si phase is fragmented into small round-shape particles due to the reduction of the total Al/Si interfacial energy. As the solution time increases from 3 to 5 h, smaller eutectic Si particles combine to form coarse ones through the Ostwald ripening mechanism. However, when the solution time is extended to 6 h, the Si particles fracture, indicating the overburning phenomenon.

Fig. 5(f) shows the SEM morphology of the intermetallic phases labeled A and B. The corresponding EDS results, calculated based on atomic percentage, are shown in Table 1. Ratios of Fe/Si and Mg/Si are also shown in Table 1. For the point A, the Fe/Si atomic ratio of 1.06 and the Al/Si atomic ratio of 5.36 are nearly consistent with β-Fe phase. In addition, for the point B, the composition ratios of Fe/Si and Mg/Si of the round intermetallic phase are almost identical to the reported π phase, while the Al/Si ratio of 1.57 is higher than the expected 1.3. Considering the size of the interaction volume created by the electron beam during the EDS analysis, the influence of the elements from the surrounding aluminum matrix has to be removed. Based on the approach [25] and the results obtained by Yao and Taylor [26] for intermetallic phase identification, these intermetallic phases could be β-$Al_5FeSi$ (marked as A) and π-$Al_8FeMg_3Si_6$ (marked as B). For composition determination with improved accuracy for these intermetallic phases in TEM, a thin foil standard with a composition close to the current phases would be required. The morphology of π-$Al_8FeMg_3Si_6$ phase particles in the as-rheocast state has transformed from needle-like to discrete rounded particles, while the needle-like β-$Al_5FeSi$ phase particles remain in close proximity to the π-$Al_8FeMg_3Si_6$ phase particles, but do not directly contact with them. This suggests that the β-$Al_5FeSi$ phase likely formed through a process of dissolution followed by reprecipitation, rather than direct transformation form π-Fe to β-Fe.

In addition, the dissolution of the π-$Al_8FeMg_3Si_6$ phase and the growth of the β-$Al_5FeSi$ phase are observed during solution treatment. The quantitative results of the π-phase and the β-phase were analyzed statistically. Fig. 6 compares the number of occurrences of the π-$Al_8FeMg_3Si_6$ phase and the β-$Al_5FeSi$ phase for different solution times, considering a field of view of about $2.8 \times 10^5$ μm$^2$. As the solution time increases, the number of the β-$Al_5FeSi$ phase gradually increases from ~150 in the as-rheocast state to ~325 after 6 h whereas the number of the π-$Al_8FeMg_3Si_6$ phase decreases from ~200 in the as-rheocast state to ~50. Zhao et al. [22] compared the number

**Table 1 – EDS quantitative results for two phases shown in Fig. 5(a) (at %).**

| Locations | Al | Si | Fe | Mg | Fe/Si | Mg/Si | Phase |
|---|---|---|---|---|---|---|---|
| A | 72.04 | 13.43 | 14.23 | 0.30 | 1.06 | – | β-$Al_5FeSi$ |
| B | 47.58 | 30.78 | 6.11 | 15.53 | 0.198 | 0.50 | π-$Al_8FeMg_3Si_6$ |

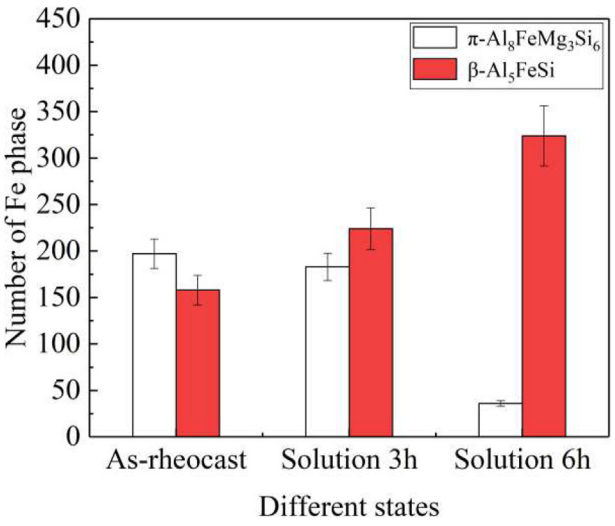


**Fig. 6 – Number of Fe-rich intermetallic phases in the alloy for various solution times.**

and volume fraction of Fe-rich intermetallic with different Fe content, and found that the trends are similar. Accordingly, we assume that the volume fraction of β-$Al_5FeSi$ phase increases with solution time, in this study. The volume fraction of the Fe-rich intermetallic phases is affected by both the Fe content [27] and the cooling rate [28]. Taylor et al. [29] pointed out that the solution treatment causes the transformation of π-$Al_8FeMg_3Si_6$ phase to the small clustered β-$Al_5FeSi$ phase when the Mg content is low (0.3–0.4 wt%). In our case, during the solution treatment process of the alloy from its as-rheocast condition, it is possible for the Mg content in the matrix around the π-$Al_8FeMg_3Si_6$ phase to reduce, causing the dissolution of π-$Al_8FeMg_3Si_6$ phase and releasing Mg, Si, and Fe into the aluminum matrix. As the diffusion coefficient of Fe in Al is less than that of Mg in Al, the local Fe content is likely to remain relatively high even as the Mg content reduces. Then, the β-$Al_5FeSi$ phase forms and grows during the dissolution of π-$Al_8FeMg_3Si_6$ phase.

The elements distribution after ageing was analyzed by EPMA, and the results are shown in Fig. 7. The elements (Si and Mg) distribution changed significantly (compared with Fig. 4). It is obvious that the β-$Al_5FeSi$ phase in bright white segregates with Fe and Si. Fig. 7(c) shows that the average concentration of Si. The decrease in Si content in the surrounding matrix, compared to the as-rheocast condition, is a result of the precipitation of Si particles during heat treatment. Similar results were also observed for Al-7Si-Mg [30] and Al-9Si-3Cu [13] alloys. In addition, the average concentration of Mg in the matrix increases owing to the dissolution of Mg-containing phases, as presented in Fig. 7(e). The artificial ageing treatments induce no visible microscale effects in the alloy. Therefore, precipitation in the aged specimens was determined using bright field imaging and selected area electron diffraction (SAED) analysis on TEM. Fig. 8 shows the bright-filed TEM results of the as-rheocast alloy and the alloy treated at 540 °C for 3 h, followed by ageing at 170 °C. Compared with the alloy in the as-rheocast state (Fig. 8(a)),

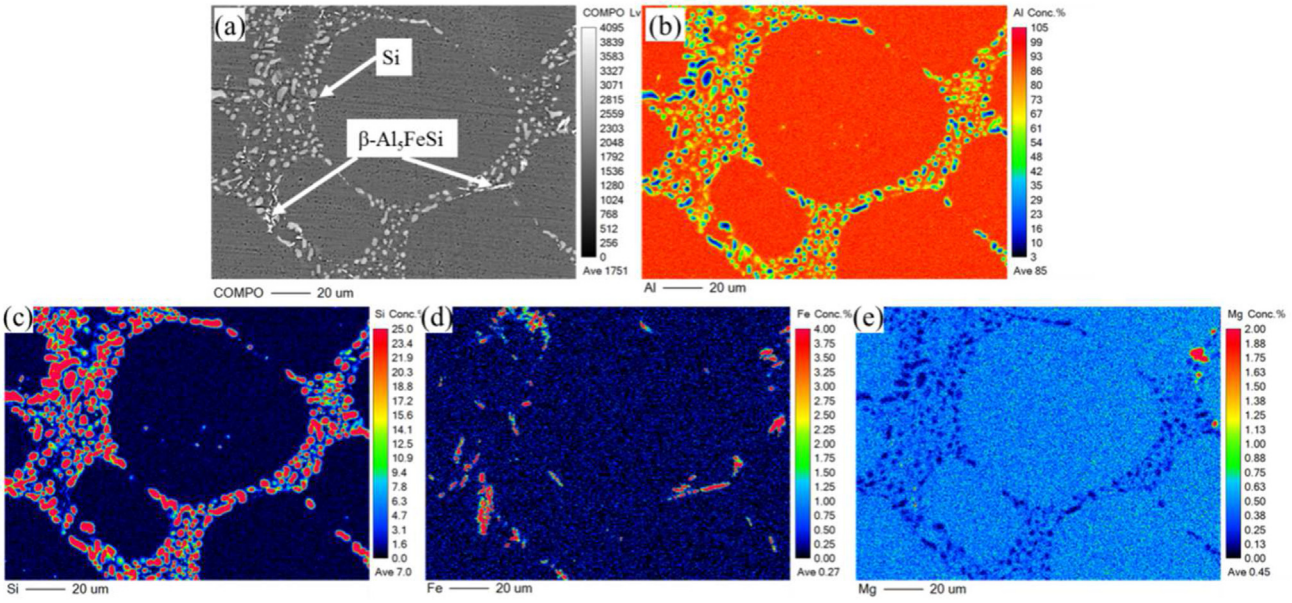


**Fig. 7 – (a) SEM back-scattered electron image; (b–e) EPMA results of the distribution of Al, Si, Fe and Mg in the alloy solution treated at 540 °C for 3 h and aged at 170 °C for 5 h.**

a lesser dislocation density is observed in the heat-treated alloy (Fig. 8(b)). In the rheo-HPDC process, the solidification of semi-solid slurry may introduce plastic deformation when external pressure is applied, leading to the formation of additional dislocations. Under higher magnification, a large number of gray precipitates with spherical morphology (diameter ~ 2–3 nm) are evenly distributed, as shown in Fig. 8(c). Typical precipitates were selected for HRTEM analysis (Fig. 8(d) and (e)) show [1 0 0] zone axis of α-Al matrix in the aged sample. There are no extra spots other than those from the α-Al matrix suggesting that fine precipitates shown in Fig. 8(c) are GP zone precipitates with the same crystal

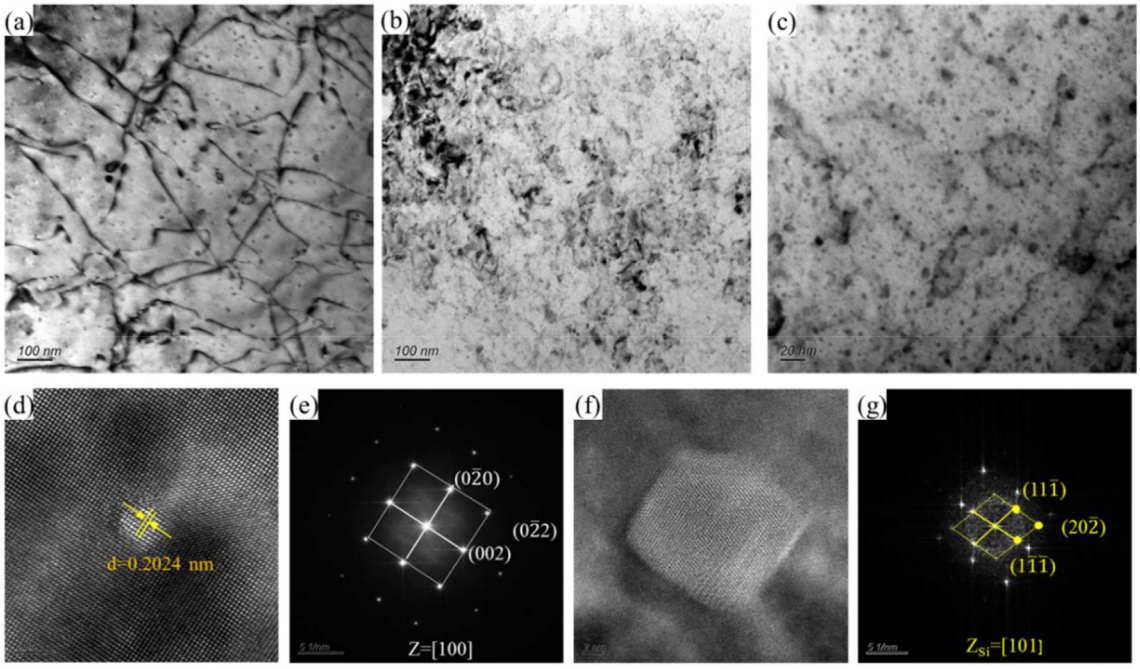


**Fig. 8 – TEM micrographs of the alloy at different conditions: (a) as-rheocast state, (b) T6 heat-treated state with (c) a higher magnification in (b), (d) and (f) showing the HRTEM micrograph of GP zone and Si dispersoids, (e) and (g) presenting the SAED patterns of GP zone and Si respectively.**

structure as that of the matrix. In addition, nano-sized approximately quadrilateral Si particles with an average length of ~6 nm are also identified, as shown in Fig. 8(g).

### 3.3. *Mechanical properties*

Fig. 9(a) shows the evolution of the microhardness in the matrix as a function of time. At the solution temperature of 540 °C, the hardness increases with solution time until a peak at 3 h, and then decreases with further increase in solution time. The increase is due to the solid solution hardening caused by the high solubility of Mg and Si at elevated temperatures, whereas the decrease after 3 h is due to the decline in solute concentration and coarsening of Si particles. Based on these findings, the present study selected the solution condition of 540 °C for 3 h to further investigate the age-hardening effect on the alloy. The age-hardening behavior at 170 °C is also presented in Fig. 9(a). The microhardness increases first and then decreases with increasing ageing time. The maximum hardness (110 ± 2 HV) of the aged alloy was attained by ageing 170 °C for 5 h. Fig. 9(b) displays the stress-strain curves of the alloy in different states, and Table 2 compares the mechanical properties for the alloys with similar chemical compositions under different forming processes and different heat treatment processes. The yield strength and ultimate tensile strength of the heat-treated alloy are significantly higher than those of the alloy in the as-rheocast state: they are 266 MPa and 343 MPa, respectively, which improves by 166% and 56% in comparison with the as-rheocast state. The fracture morphology observation was performed on the tensile samples after failure. Fig. 10 shows the fracture surfaces of the alloy under different processing conditions. They mainly consist of tear ridges and dimples with some quasi-cleavage zones.

## 4. Discussion

### 4.1. *Segregation behavior*

Because of the characteristics of the semi-solid slurry, segregation is hard to eliminate in the rheo-HPDC process. Especially, a surface liquid segregation phenomenon is prone to occur, which is strongly affected by alloy composition, die geometry and processing parameters [38]. In this study, we examined the microstructure of one part in different zones, as shown in Fig. 3. The results of the image analysis in various zones show that there are surface liquid segregation zones (zones 2, 5 and 7). As compared to zone 1, the obvious surface liquid segregation phenomenon in zone 2 is thought to be related to the filling length. Zabler et al. [39] have argued from in situ observations that the liquid was pushed to the flow front of the slurry, and since it is much more fluid than solid grains, it results in an increase of the liquid fraction in the upper zone of the part (e.g. zone 2). The segregation could be more severe for longer filling length, as it was also stated by Feng et al. [40]. In addition, the surface liquid segregation was observed in the corner of the part (zones 5 and 7). Generally, segregation increases when the flow direction is changed or when the flow passes through an abrupt change of the free cross-section [41]. As previously mentioned, the liquid phase is pushed towards the edge, causing an increase in liquid fraction on the surface. When the material flows to zone 7, the high velocity of the piston can cause the slurry to detach from the corner wall of the die. The slurry flows along the horizontal duct to the left wall of the core, and then the slurry is turned around and flows back to the center of the die. The small gap caused by the detachment would be subsequently filled during the filling process. As a consequence, the remixing of liquid segregation becomes evident in zone 7. The liquid segregation phenomenon in zone 5 may also result from the detachment of the slurry that may be reduced by decreasing injection velocity according to the results of Hufschmidt et al. [42]. Based on the microstructure and the statistic results of liquid fraction in zones 4 and 6, the segregation of solid could be deduced. When the material flows into zones 4 and 6, the liquid phase is squeezed out, resulting in a low liquid fraction. Except for the surface segregation zones, no appreciable difference is observed between the microstructure inside the part. These results suggest that the geometry of the die and the piston velocity affect segregation. As mentioned in Gu et al. [43] and Neag et al. [44] for thixoforming of steels and aluminium alloys, the macro liquid segregation seems to require a high enough amount of free liquid. Therefore, it is very interesting to investigate the effects of processing temperature on the liquid fraction in the near future.

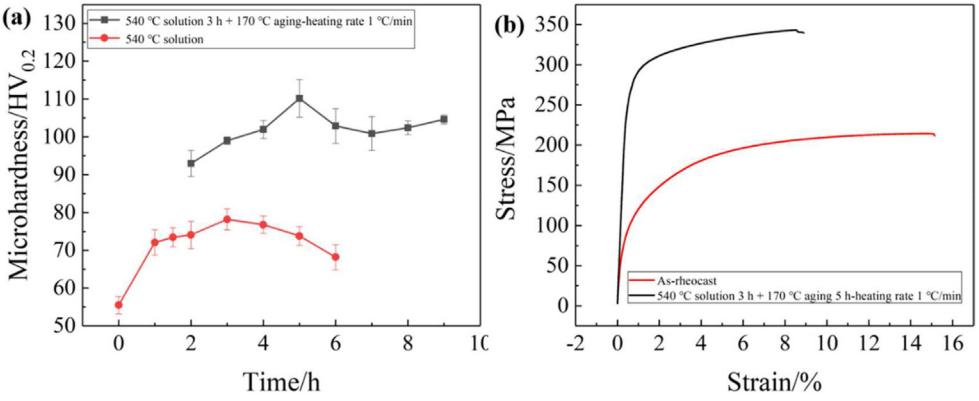


**Fig. 9 – Microhardness evolution as a function of solution time and ageing time.**

**Table 2 – Comparison of mechanical properties for several Al-Si based alloys.**

| Alloys | Forming process | UTS-YS-EL MPa-MPa-% | Solution | Ageing | References |
|---|---|---|---|---|---|
| Al-7Si-0.2Fe-0.4Mg-0.3Cu-0.02Mn-0.27Mo-0.16Zn-0.17Zr | Water-cooled copper mold casting | 275-139-7.9 | – | – | [1] |
| Al-8.2Si-0.53Fe-0.46Mg-0.15Cu-0.01Sr | HPDC | 208.7-129.5-2.2 | – | – | [21] |
| Al-8.2Si-0.53Fe-0.46Mg-0.15Cu-0.01Sr | Semi-solid die-casting | 358.2-279.9-12.5 | 535 °C-1h | 170°C-2.5h | [31] |
| Al-8.2Si-0.53Fe-0.46Mg-0.15Cu-0.01Sr | Semi-solid die-casting | 293.1-146.7-9.8 | | | [32] |
| Al-7Si-0.6Mg-0.13Fe-0.13Ti | Sand casting | 312-301-0.6 | 550°C-2h | 180°C-22h | [33] |
| Al-7Si-0.4Mg-0.5Sc | casting | 331-263-12 | 535°C-4h | 150°C-10h | [34] |
| Al-7Si-0.4Mg-0.2Ti-0.13Fe-0.1Cu | Semi-solid squeeze casting | 283-201-8 | 540°C-3h | 160°C-9h | [35] |
| Al-7Si-0.4Mg-0.1Fe | Semi-solid die-casting | 293–/–10.21 | 540°C-8h | 160°C-8h | [36] |
| Al-7Si-0.3Mg-0.1Ti-0.1Fe | Low pressure casting | 285-210-14.0 | 540°C-4h | 155 °C -3h | [37] |

### 4.2. *Improvement of mechanical properties*

In general, the static strength depends on the relative density as well as the microstructure formed during rheo-HPDC. As compared to the part processed by traditional HPDC, the reduced defects shown in Fig. 2 and the uniformly distributed α-Al grains (shown in Fig. 3) can transfer the external force to more grains during tension, resulting in a larger elongation. In addition, the yield strength and the tensile strength of the alloy are improved by heat treatment, as compared to those in the as-rheco-HPDC state. This may be related to both solution and precipitation strengthening. Si atoms in the α-Al matrix tend to diffuse toward the Si particles during the heat treatment, leading to a decrease in Si concentration in α-Al matrix. However, the concentration of Mg atoms in the matrix increases significantly due to the dissolution of Mg-containing phases (Fig. 7). Chen et al. [30] suggested that solution strengthening effect of Mg is much stronger than that of Si. Leyson et al. [45] also stated that the Mg hardening effect is twice higher than that of Si, because of the smaller size misfit and modulus misfit of Si in the Al matrix. With regard to the ageing process, the fine particles precipitate from the supersaturated solid solution and hinder the movement of dislocations, resulting in the enhancement of the strength as well. After ageing treatment, the combination of GP zones and well-dispersed semi-coherent precipitates in the matrix plays a

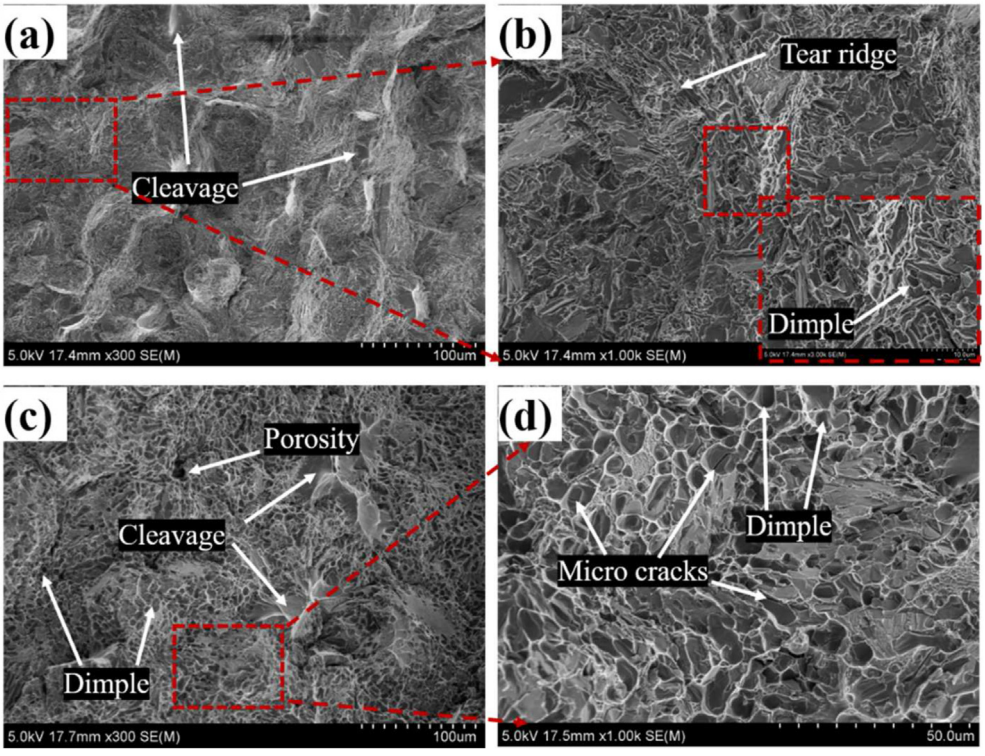


**Fig. 10 – Fracture morphology of A356 in the as-rheocast state (a), solution treated at 540 °C for 3 h (b) and aged at 170 °C for 5 h (c) and (d).**

role in precipitation strengthening of the alloy. Furthermore, the morphology of intermetallic phases and eutectic Si phases has an effect on the elongation. After heat treatment, the refined fibrous eutectic Si phases decreases the crack propagation rate, while the increase of needle-like β-$Al_5FeSi$ phase content may increase the stress concentration during tensile test. In addition to the microstructure, the elongation is closely associated with the voids. As shown in Fig. 10, porosities in the heat-treated samples were observed, which may decrease the elongation of the alloy.

## 5. Conclusions

A356 aluminium components with complex shape were successfully fabricated by rheo-HPDC process with the SEED method for semi-solid preparation. The segregation, microstructure and mechanical properties were investigated. Based on the analysis and discussion of the results, the conclusions are as follows:

(1) A quasi defect-free component could be obtained by rheo-HPDC process. The alloys are composed of spherical primary α-Al grains (average size is ~95 μm) and secondary solidified α-Al grains divided by eutectic Si and iron-rich intermetallic phases.
(2) Liquid segregation occurred in the upper zone of the part because of long filling length and in the corner of the part because of die geometry, while homogeneous microstructure inside the part can be obtained.
(3) As compared with the samples in the as-rheocast state, the T6 treated samples (solution at 540 °C for 3 h and artificial aged at 170 °C for 5 h) exhibit excellent mechanical properties, because of the solution strengthening and precipitation strengthening mechanisms. The T6 treated samples have a yield strength of 266 MPa and an ultimate tensile strength of 343 MPa. The rheo-HPDC samples exhibit a mixed-fracture mechanism of dimple and quasi-cleavage fracture in both the as-rheocast and heat-treated states. Heat treatment causes the script-like π-$Al_8FeMg_3Si_6$ intermetallic phases to transform into needle-like β-$Al_5FeSi$ phase, which may decrease stress cracking resistance and result in a decrease in elongation of the T6 treated samples.

## Declaration of competing interest

The authors declare that they have no known competing financial interests or personal relationships that could have appeared to influence the work reported in this paper.

## Acknowledgments

This work was supported by the Key Research and Development Program of Shandong Province (2021ZLGX01 and 2020CXGC010305), the Natural Science Foundation of Jiangsu Province (BK20160369), National Natural Science Foundation of China (No. 51705292), Natural Science Foundation of Shandong Province (ZR201702180340).

## REFERENCES

[1] Zou J, Zhang H, Yu C, Wu Z, Guo C, Nagaumi H, et al. Investigating the influences of Fe, Mn and Mo additions on the evolution of microstructure and mechanical performances of Al-Si-Mg cast alloys. J Mater Res Technol 2023;25:319–32. https://doi.org/10.1016/j.jmrt.2023.05.234.
[2] Mao GL, Zhu CC, Wang S, Yan H, Gao WL. The role of yttrium modifying A357 alloy with sand casting. Mater Sci Technol 2019;35(6):1815–21. https://doi.org/10.1080/02670836.2019.1650442.
[3] Khaled AR, Mohamed B. X.-Grant C Quality index charts of Al-Si-Mg semi solid alloys subjected to multiple temperatures aging treatments and different quenching media. Materials 2019;12(11):1834. https://doi.org/10.3390/ma12111834.
[4] Ragab KA, Bouazara M, Bouaicha A, Allaoui O. Microstructural and mechanical features of aluminium semi-solid alloys made by rheocasting technique. Mater Sci Technol 2017;33(6):646–55. https://doi.org/10.1080/02670836.2016.1216263.
[5] Kirkwood DH, Suéry M, Krapanos P, Atkinson HV, Young KP. Semi-solid processing of alloys. Berlin: Springer-verlag; 2016. ISBN 978-3-642-00706-4.
[6] Nafisi S, Ghomashchi R. Semi-solid processing of aluminum alloys. Berlin: Springer International Publishing Switzerland; 2016. ISBN 978-3-319-40333-5.
[7] Honarmand M, Salehi M, Shabestari SG, Saghafian H. Impact strength and structural refinement of A380 aluminum alloy produced through gas-induced semi-solid process and Sr addition. T Nonferr Metal Soc 2022;32(5):1405–15. https://doi.org/10.1016/S1003-6326(22)65882-5.
[8] Haga T, Kapranos P. Simple rheocasting processes. J Mater Process Technol 2002;130–131:594–8. https://doi.org/10.1016/S0924-0136(02)00819-1.
[9] Lin C, Wu SS, Lü SL, An P, Wan L. Microstructure and mechanical properties of rheo-diecast hypereutectic Al-Si alloy with 2%Fe assisted with ultrasonic vibration process. J Alloys Compd 2013;568:42–8. https://doi.org/10.1016/j.jallcom.2013.03.089.
[10] Doutre D, Hay G, Wales P. Semi-solid concentration processing of metallic alloys. US Patent, No. 6 August 2002;6(428):636.
[11] Li G, Qu WY, Luo M, Cheng L, Guo, Li XG, et al. Semi-solid processing of aluminum and magnesium alloys: status, opportunity, and challenge in China. T Nonferr Metal Soc 2021;31(11):3255–80. https://doi.org/10.1016/S1003-6326(21)65729-1.
[12] Liang XK. Study on manufacturing technology and application of semi-solid slurry of Al-Si alloys [D.Eng dissertation]. Beijing: General research institute for nonferrous metals; 2017.
[13] Luo M, Li DQ, Midson SP, Qu WY, Zhu Q, Fan JZ. Model for predicting radial temperature distribution of semi-solid slug produced by swirled enthalpy equilibration device (SEED) process. J Mater Process Technol 2019;273:116236. https://doi.org/10.1016/j.jmatprotec.2019.05.017.
[14] Menargues S, Martín E, Baile MT, Picas JA. New short T6 heat treatments for aluminium silicon alloys obtained by semisolid forming. Mater Sci Eng, A 2015;621:236–42. https://doi.org/10.1016/j.msea.2014.10.078.

[15] Fabrizi A, Capuzzi S, Alessandro DM, Timelli G. Effect of T6 heat treatment on the microstructure and hardness of secondary AlSi9Cu3(Fe) alloys produced by semi-solid SEED process. Metals 2018;8(10):750. https://doi.org/10.3390/met8100750.
[16] Ridvan G, Serhat A, Alptekin K, Kerem AG, Ahmet K. Influence of T6 heat treatment on A356 and A380 aluminium alloys manufactured by thixoforging combined with low superheat casting. T Nonferr Metal Soc 2018;28(3):385–92. https://doi.org/10.1016/S1003-6326(18)64672-2.
[17] Shabestari SG, Abdi M, Naghdali S. Effect of thixoforming and precipitation hardening on microstructure and mechanical properties of Al-10.5Si–3Cu-0.2Mg alloy produced by strain induced melt activation process. J Mater Res Technol 2021;15:4981–92. https://doi.org/10.1016/j.jmrt.2021.10.086.
[18] Gu GC, Xiang LX, Li RF, Xu WH, Lu Yp Pesci R. Effects of process parameters on microstructure and mechanical properties of semi-solid Al-7Si-0.5Mg aluminum alloy by gas induced semi-solid process. Metals 2022;12(10):1600. https://doi.org/10.3390/met12101600.
[19] Ohno A. Solidification—the separation theory and its practical applications. first ed. Berlin: Springer; 1987.
[20] Qu W, Luo M, Guo Z, Hu X, Zhang A, Zhang F, et al. Microstructural evolution mechanism of semi-solid slurry: a study using Phase-Field-Lattice-Boltzmann scheme. J Mater Res Technol 2020;280:116592. https://doi.org/10.1016/j.jmatprotec.2020.116592.
[21] Liu Y, Gao MQ, Meng SC, Fu Y, Li WR, Li CH, et al. Solidification behavior and enhanced properties of semi-solid Al-8Si-0.5Fe alloys fabricated by rheo-diecasting. J Mater Res Technol 2022;19:3160–71. https://doi.org/10.1016/j.jmrt.2022.06.062.
[22] Zhao JH, Xu B, Gu C, Wang YJ, Tang Q. Effect of microstructure evolution of iron-rich intermetallic compounds on mechanical property of Al–7Si–0.3Mg casting alloy with low iron content. Metall Mater Trans B 2022;53:548–60. https://doi.org/10.1007/s11663-021-02390-5.
[23] Wang QG, Davidson CJ. Solidification and precipitation behaviour of Al-Si-Mg casting alloys. J Mater Sci 2001;36:739–50. https://doi.org/10.1023/A:1004801327556.
[24] Payandeh M, Sjölander E, Jarfors AEW, Wessén M. Influence of microstructure and heat treatment on thermal conductivity of rheocast and liquid die cast Al-6Si-2Cu-Zn alloy. Int J Cast Metals Res 2016;29(4):202–13. https://doi.org/10.1080/13640461.2015.1125990.
[25] Qian M, Taylor JA, Yao JY, Couper MJ, StJohn DH. A practical method for identifying intermetallic phase particles in aluminum alloys by electron probe microanalysis. J Light Met 2001;1(3):187–93. https://doi.org/10.1016/S1471-5317(01)00012-8.
[26] Yao JY, Taylor JA. Characterisation of intermetallic particles formed during solution treatment of an Al-7Si-0.4Mg-0.12Fe alloy. J Alloys Compd 2012;519:60–6. https://doi.org/10.1016/j.jallcom.2011.12.047.
[27] Sweet L, Zhu SM, Gao SX, Taylor JA, Easton MA. The effect of iron content on the iron-containing intermetallic phases in a cast 6060 aluminum alloy. Metall Mater Trans A 2011;42:1737–49. https://doi.org/10.1007/s11661-010-0595-6.
[28] Gorny A, Manickaraj J, Cai ZH, Shankar S. Evolution of Fe based intermetallic phases in Al–Si hypoeutectic casting alloys: influence of the Si and Fe concentrations, and solidification rate. J Alloys Compd 2013;577:103–24. https://doi.org/10.1016/j.jallcom.2013.04.139.
[29] Taylor JA, Stjohn DH, Barresi J, Couper MJ. Influence of Mg content on the microstructure and solid solution chemistry of Al-7%Si-Mg casting alloys during solution treatment. Mater Sci Forum 2000;331:277–82. https://doi.org/10.4028/www.scientific.net/MSF.331-337.277.
[30] Chen R, Xu QY, Jia ZN, Liu BC. Precipitation behavior and hardening effects of Si-containing dispersoids in Al-7Si-Mg alloy during solution treatment. Mater Des 2016;90:1059–68. https://doi.org/10.1016/j.matdes.2015.11.069.
[31] Liu Y, Chen XL, Gao MQ, Guan RG. Enhanced strength-ductility synergy in a rheo-diecasting semi-solid aluminum alloy. Mater Lett 2021;305:130756. https://doi.org/10.1016/j.matlet.2021.130756.
[32] Liu Y, Meng SC, Gao MQ, Pan S, Fu Y, Guan RG. Enhanced comprehensive performance via alloying and rheo-diecasting in a semi-solid Al–Si–Fe–Mg–Cu–Sr alloy. J Mater Res Technol 2023;25:420–39. https://doi.org/10.1016/j.jmrt.2023.05.222.
[33] Rui C, Xu Q, Guo H, Xia Z, Liu B. Correlation of solidification microstructure refining scale, Mg composition and heat treatment conditions with mechanical properties in Al-7Si-Mg cast aluminum alloys. Mater Sci Eng, A 2016;685:391–402. https://doi.org/10.1016/j.msea.2016.12.051.
[34] Liu GC, Gao JB, Che C, Lu Z, Yi W, Zhang LJ. Optimization of casting means and heat treatment routines for improving mechanical and corrosion resistance properties of A356-0.54Sc casting alloy. Mater Today Commun 2020;24(1):101227. https://doi.org/10.1016/j.mtcomm.2020.101227.
[35] Cheng L, Lu HX, Zhu Q, Zhang XK, Shen AD, Yang P. Evolution of microstructure and mechanical properties of semi-solid squeeze cast A356.2 aluminum alloy during heat treatment. Solid State Phenom 2019;285:139–45. https://doi.org/10.4028/www.scientific.net/SSP.285.139.
[36] Thanabumrungkul S, Janudom S, Burapa R, Dulyapraphant P, Wannasin J. Industrial development of gas induced semi-solid process. T Nonferr Metal Soc 2010;20:1016–21. https://doi.org/10.1016/S1003-6326(10)60623-1.
[37] Yang BC, Chen SF, Song HW, Zhang SH, Chang HP, Xu SW, et al. Effects of microstructure coarsening and casting pores on the tensile and fatigue properties of cast A356-T6 aluminum alloy: a comparative investigation. Mater Sci Eng, A 2022;857:144106. https://doi.org/10.1016/j.msea.2022.144106.
[38] Möller H, Curle UA, Masuku EP. Characterization of surface liquid segregation in SSM-HPDC aluminum alloys 7075, 2024, 6082 and A201. Trans Nonferrous Metals Soc China 2010;20:847–51. https://doi.org/10.1016/S1003-6326(10)60593-6.
[39] Zabler S, Ershov A, Rack A, Garcia-Moreno F, Baumbach T, Banhart J. Particle and liquid motion in semi-solid aluminium alloys: a quantitative in situ microradioscopy study. Acta Mater 2013;61(4):1244–53. https://doi.org/10.1016/j.actamat.2012.10.047.
[40] Feng J, Liu ZK, Li DQ, Zhu JH, Chen S, Zhang F. Evolution of segregation, microstructure and mechanical properties of a semisolid die casting Al-6Si-3Cu-0.4Mg alloy. International Journal of Lightweight Materials and Manufacture 2023;6(2):245–53. https://doi.org/10.1016/j.ijlmm.2022.11.002.
[41] Adriana N, Favier V, Bigot R, Atkinsond HV. Comparison between numerical simulation of semisolid flow into a die using Forge and in situ visualization using a transparent sided die. J Mater Res Technol 2016;229:338–48. https://doi.org/10.1016/j.jmatprotec.2015.09.035.
[42] Hufschmidt M, Modigell M, Petera J. Modelling and simulation of forming processes of metallic suspensions under non-isothermal conditions. J Non-Newtonian Fluid Mech 2006;134(1–3):16–26. https://doi.org/10.1016/j.jnnfm.2005.10.006.

[43] Gu G, Pesci R, Langlois L, Becker E, Bigot R. Microstructure investigation and flow behavior during thixoextrusion of M2 steel grade. J Mater Process Technol 2015;216:178–87. https://doi.org/10.1016/j.jmatprotec.2014.09.009.

[44] Neag A, Favier V, Bigot R, Pop M. Microstructure and flow behaviour during backward extrusion of semi-solid 7075 aluminium alloy. J Mater Process Technol 2012;212(7):1472–80. https://doi.org/10.1016/j.jmatprotec.2012.02.003.

[45] Leyson GPM, Hector Jr LG, Curtin WA. Solute strengthening from first principles and application to aluminum alloys. Acta Mater 2012;60(9):3873–84. https://doi.org/10.1016/j.actamat.2012.03.037.